energies

Article

Hydrothermal Conversion of Microalgae Slurry in a Continuous Solar Collector with Static Mixer for Heat Transfer Enhancement

Hao Chen, Fangfang Lou, Xueyi Zhang, Chengjun Shen, Weicheng Pan and Shuang Wang *

School of Energy and Power Engineering, Jiangsu University, Zhenjiang 212013, China; haochen@ujs.edu.cn (H.C.); 18786272304@163.com (F.L.); zhangxueyisakura@163.com (X.Z.); sdlysdj2002@163.com (C.S.); pan3312833572@163.com (W.P.)
* Correspondence: alexjuven@ujs.edu.cn

Abstract: The continuous solar collector is a promising heater and reactor for the hydrothermal liquefaction (HTL) of microalgae biomass. To enhance the heat transfer and hydrothermal conversion of microalgae slurry in solar-driven reactors, a static mixer is inserted in the flow channel of the solar collector. A numerical model combining CFD and HTL reactions of microalgae biomass is proposed. Six composition equations of protein, carbohydrates, lipids, biocrude, aqueous phase and biogas were proposed, while corresponding HTL kinetics were utilized to simulate the conversion rate of the reactants and products. The effects of the twist ratio of the static mixer (3–10), flow rate (30–80 L/h) and solar intensity (650, 750, 850 W/m^2) on the flow resistance, heat transfer and organics formation of microalgae slurry were investigated. The swirl flow caused by the static mixer with a twist ratio of three increased the convective heat transfer coefficient (97 W·m^{-2}·K^{-1}) by 2.06 times, while the production rate of biocrude (0.074 g·L^{-1}·s^{-1}) increased by 2.05 times at 50 L/h and 750 W/m^2. This investigation gives guidance for utilizing static mixers in solar-driven reactors to optimize the heat transfer and HTL of microalgae biomass with solar heat sources.

Keywords: microalgae biomass; solar collector; static swirler; biocrude yield; heat transfer enhancement; CFD and HTL kinetics

check for updates

Citation: Chen, H.; Lou, F.; Zhang, X.; Shen, C.; Pan, W.; Wang, S. Hydrothermal Conversion of Microalgae Slurry in a Continuous Solar Collector with Static Mixer for Heat Transfer Enhancement. *Energies* **2023**, *16*, 7986. https://doi.org/10.3390/en16247986

Academic Editors: Tapas Mallick and Anastassios M. Stamatelos

Received: 27 September 2023
Revised: 20 October 2023
Accepted: 15 November 2023
Published: 9 December 2023

Copyright: © 2023 by the authors. Licensee MDPI, Basel, Switzerland. This article is an open access article distributed under the terms and conditions of the Creative Commons Attribution (CC BY) license (https://creativecommons.org/licenses/by/4.0/).

1. Introduction

Biofuel is regarded as carbon-neutral energy and has drawn great attention due to its zero CO_2 emissions [1–3]. Microalgae biomass is an attractive source of biofuel to substitute for conventional fossil fuels, due to its ability to efficiently convert CO_2 into biomass through photosynthesis in cultivation [4,5]. Thermochemical processes, such as combustion, pyrolysis, gasification and hydrothermal conversion, are a promising route for biofuel production [6,7]. Particularly, hydrothermal conversion converts wet biomass into biofuels in hot-compressed water [8,9], reducing energy consumption during the dry process [10]. As microalgae biomass exists in algal slurry with high water content, hydrothermal conversion acts as a suitable method to produce microalgal biofuels [11,12]. For instance, biocrude oils containing ideal heating values (36–40 MJ/kg) are obtained from microalgae using hydrothermal liquefaction (HTL) [13].

The combination of solar collectors and continuous HTL reactors is a promising route to establish zero-energy consumption systems for biofuel production [14,15]. Solar energy, as a renewable and economical heat source, is utilized to supply the heating requirement of microalgae biomass in HTL reactors. To satisfy the temperature conditions (250–350 °C) of HTL [16], several concentrated solar collectors, such as parabolic trough solar collectors and dish solar collectors, are utilized to directly heat the feedstocks during the HTL process [17,18]. Giaconia et al. [19] analyzed an HTL system to produce biocrude from microalgae; parabolic solar collectors and electric power were utilized to support the heat requirement of the HTL system. Saucedo et al. [20] proposed a novel solar reactor for hydrothermal processing, containing a solar cavity receiver and seven tubes for biomass slurry flow. Briongos et al. [21] proposed a linear solar-driven reactor with twin-screws for continuous hydrothermal carbonization of wet biomass. The effects of the incoming heat flux (8–20 kW/m^2), reactor length (L/D = 30–60) and the rotating velocity of the screw (25–100 rpm) were investigated. Xiao et al. [17] established a parabolic solar-driven continuous hydrothermal reactor for algal biomass, in which the processing capacity of the microalgae was set at 60 L/h.

Due to the weak heat conductivity of biomass slurry, the high temperature gradient of algal slurry in the continuous reactor is the bottleneck of the HTL process [22–24]. Fu et al. [25] indicated that the thermal conductivity of the cell of *Chlorella* is 0.512 W·m^{-1}·K^{-1} at 25 °C, which is obviously lower than water (0.62 W·m^{-1}·K^{-1}). In a tubular reactor with uniform heat flux, the radial temperature difference is higher than 60 °C, inducing a negative effect on the HTL of the algal biomass [25]. As the solar-integrated reactor receives non-uniform heat fluxes reflected by the solar reflector, the temperature heterogeneity of the algal slurry in the solar reactor is higher than that in the tubular reactor with a uniform heat flux [23]. For instance, the non-uniform heat flux in the circumferential direction of the solar collector can produce a temperature difference higher than 30 °C, while the temperature difference of algal slurry is higher than 50 °C at a flow rate of 60 L/h [24]. During the HTL process, the reaction rate and the composition of products are significantly affected by the temperature [16]. Therefore, it is urged for the heat transfer of algal slurry to be reinforced for enhancing the solar-driven HTL process.

Twisted tape is an efficient device that is inserted in tubular reactors for the enhancement of the heat transfer of fluid [26,27]. Regarding biomass slurry as a heat transfer fluid, high viscosity limits its heat transfer enhancement. Twisted tape inserted in the heat transfer can give rise to the swirl effect and reduce the thermal boundary layer thickness of heat transfer fluid in the tube [28,29], enhancing the convective heat transfer performance. Moreover, algal slurry is a non-Newtonian fluid, causing the appearance of shear-thinning properties [30]. Therefore, the swirl effect of algal slurry is able to reduce the viscosity, further enhancing the heat transfer of algal slurry [27]. Recently, static mixers are increasingly being utilized in heat transfer process industries [31]. The Nusselt numbers of tubes with static mixers are three times higher than plain tubes, while the twist ratio of the static mixer is between 3 and 10 [32]. In addition, the high-efficiency mixing induced by static mixers is beneficial to optimize the mass transfer in the continuous reactor during chemical conversion [33,34]. Chen et al. proposed a tubular reactor with a static mixer [24]; the convective heat transfer coefficient (1707 W·m^{-2}·K^{-1}) and biocrude yield (0.298 g·L^{-1}) were 2.55 and 1.59 times higher than those of a plain tubular reactor [22]. In general, the heat transfer performance of fluid in the tube flow with static mixers has been discussed in detail. However, the HTL of biomass slurry in tubular reactors with non-uniform heat resources has not been clearly investigated. Therefore, the heat transfer enhancement of algal slurry in solar-driven HTL reactors with static mixers deserves to be investigated.

In this study, a numerical model combining flow, heat transfer, HTL kinetics and non-uniform heat boundary conditions is proposed. The effects of the twist ratio of the static mixer (3–10), flow rate (30–80 L/h) and solar intensity (650, 750, 850 W·m^{-2}) on the flow resistance, heat transfer and the yield of organics in the HTL reactor were investigated. On this basis, the PECs of solar-driven reactors with different static mixers were compared. The swirler effects on the heat transfer and HTL conversion of algal slurry in the solar reactor were analyzed. In addition, the comprehensive effects of direct solar radiation intensity and the residence time of the algal slurry in the reactor were analyzed. This investigation gives guidance for utilizing static mixers in continuous solar reactors for the design and optimization of the continuous HTL of biomass slurry.

2. Numerical Model and Simulations

2.1. Physical Condition and Model Assumptions

Figure 1 shows the three-dimensional model of a solar-driven tubular reactor with or without a static mixer. The length (L) of the solar-driven tubular reactor was 6000 mm.

The outer diameter and inner diameter of the solar-driven tubular reactor were 38 mm and 32 mm, respectively. The length (L) and the width (w) of the parabolic trough solar reflector were 6000 mm and 2550 mm, respectively. The specular reflectance, transmission of the glass tube and absorptance of the collector were 0.93, 0.915 and 0.95, respectively. In this case, the direct solar radiation intensity was set as 650, 750 and 850 W/m^2, while the corresponding non-uniform heat flux q on the outer wall of the solar-driven tubular reactor can be expressed as Equation (1), Equation (2) and Equation (3), respectively [24].

$$q_{650\mathrm{W/m}^2} = \begin{cases} -1734.9x^2 + 41930x - 222688 & 0^\circ \le \theta \le 130^\circ \\ -65.584x^2 + 1804.3x + 17429 & 130^\circ < \theta \le 180^\circ \\ -65.584x^2 - 1804.3x + 17429 & 180^\circ < \theta \le 230^\circ \\ -1734.9x^2 - 41930x - 222688 & 230^\circ < \theta \le 360^\circ \end{cases} \tag{1}$$

$$q_{750\mathrm{W/m}^2} = \begin{cases} -2001.8x^2 + 48380x - 256946 & 0^\circ \le \theta \le 130^\circ \\ -81.652x^2 + 2139.2x + 20031 & 130^\circ < \theta \le 180^\circ \\ -81.652x^2 - 2139.2x + 20031 & 180^\circ < \theta \le 230^\circ \\ -2001.8x^2 - 48380x - 256946 & 230^\circ < \theta \le 360^\circ \end{cases} \tag{2}$$

$$q_{850\mathrm{W/m}^2} = \begin{cases} -2268.8x^2 + 54831x - 291206 & 0^\circ \le \theta \le 130^\circ \\ -92.539x^2 + 2424.5x + 22702 & 130^\circ < \theta \le 180^\circ \\ -92.539x^2 - 2424.5x + 22702 & 180^\circ < \theta \le 230^\circ \\ -2268.8x^2 - 54831x - 291206 & 230^\circ < \theta \le 360^\circ \end{cases} \tag{3}$$

where the corresponding x-axis coordinate value x (m) is calculated as follows:

$$x = 16\sin(\theta\pi/180^\circ) \tag{4}$$

where θ is the angle of the solar-driven tubular reactor.

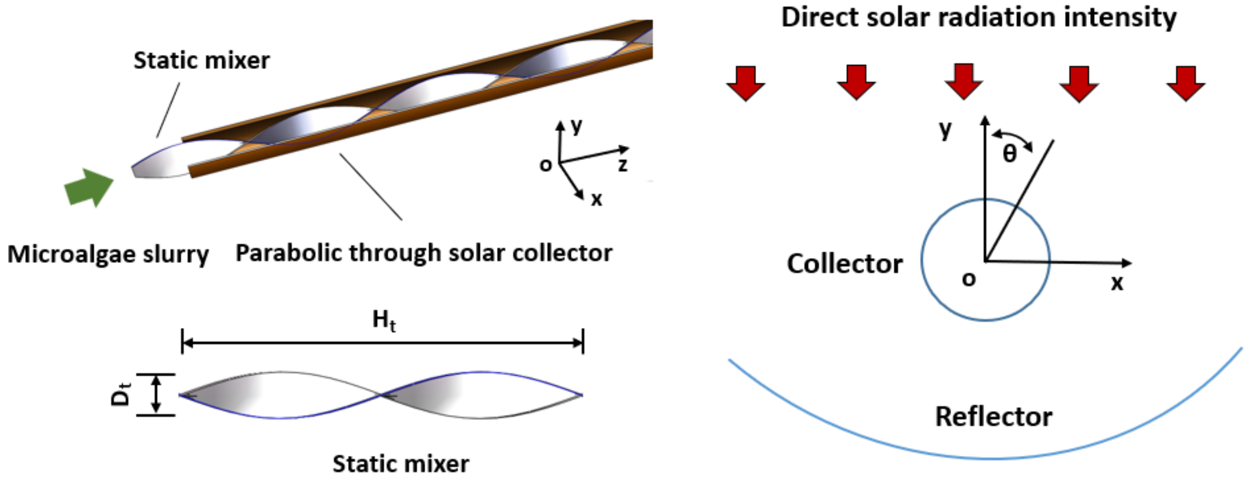

Figure 1. Schemes of parabolic trough solar-driven reactor with static mixer.

The static mixers inserted in the solar-driven tubular reactor have a series of twist ratios ($Y = H_t/D_t = 3, 4, 6, 10$), which represent the relationship between the axial distance of the static mixer (H_t) and the width of the static mixer (D_t) (shown in Figure 1). According to the twist ratio of static mixers, the static mixers were labeled as SM-3, SM-4, SM-6 and SM-10, respectively. The thickness (δ) and the width (D_t) of the static mixer were 1 mm and 28 mm, respectively.

In the continuous HTL of microalgae biomass, algal slurry was continuously flowing through the solar-driven tubular reactor with or without the static mixer. Meanwhile, the algal slurry flow through the solar-driven reactor absorbs the non-uniform heat supplied from the parabolic trough solar reflector. The flow rates of the algal slurry were set as 30, 40, 50, 60, 70, 80 L/h. The inlet temperatures of the algal slurry were set as 300 K. The algal slurry mainly contains microalgae biomass and water, whose mass fraction of microalgae biomass was set as 10 wt.%. The outlet pressure was set as 20 MPa. In general, boundary conditions and the studied parameters are summarized in Table 1.

Table 1. Boundary conditions and the studied parameters.

Boundary Condition	Value
Flow rate at the inlet	30, 40, 50, 60, 70, 80 L/h
Mean temperature at the inlet	300 K
Pressure at the outlet	20 MPa
Direct solar radiation intensity	650, 750 and 850 W/m^2
Heat flux at the wall	Equation (1), Equation (2), Equation (3)
Studied parameters	*f*, *Nu*, PEC, *Re*, yield of water-soluble organics, biocrude, biogas, formation rate of biocrude

2.2. Governing Equations

In the current study, a three-dimension model was established. The non-uniform heat flux distribution was applied around the tube, whose distribution pattern obeys Equations (1)–(3). Algal slurry was assumed as an incompressible and homogeneous fluid. With the forced convection and swirl effect, the effect of gravity on the flow process is ignored. Laminar flow pattern was set (Re < 25). There is no boundary slip on the wall of the tubular reactor. Therefore, the governing equations in a steady state were written as follows, respectively [35,36].

$$\nabla \cdot \left(\rho \vec{u}\right) = 0 \tag{5}$$

$$\nabla \cdot \left(\rho \vec{u}\,\vec{u}\right) = -\nabla P + \nabla \cdot \left(\mu\left(\nabla \cdot \vec{u} + \nabla \cdot \vec{u}^{T}\right)\right) \tag{6}$$

$$\nabla \cdot \left(\rho c_p T \vec{u}\right) = \nabla \cdot (\lambda \nabla T) \tag{7}$$

$$\nabla \cdot \left(\rho \vec{u} w_i\right) = \nabla \cdot (\mathrm{D}_i \nabla w_i) + \rho r_i \tag{8}$$

where w_i (i = 0–5) is the mass fraction of protein, carbohydrate, lipid, water-soluble organics, biocrude and gas, respectively:

$$w_i = c_i/\rho \tag{9}$$

where c_i (i = 0–5) is the concentration of several components.

In Equations (5)–(8), the density of the algal slurry ρ is expressed as follows:

$$\frac{1}{\rho} = \frac{1}{\rho_{\mathrm{s}}}\omega + \frac{1}{\rho_f}(1-\omega) \tag{10}$$

where ω is the mass fraction of dry microalgae (10 wt.%) in the slurry, ρ_s and ρ_f are the density of the dry microalgae (1324 kg/m^3) and water (kg/m^3) [37], respectively.

$$\rho_f = 834.87 + 1.39T - 0.00284T^2 \tag{11}$$

In Equation (6), the viscosity μ (Pa·s) is expressed as follows:

$$\mu = K\dot{\gamma}^{n-1} \tag{12}$$

where K is the consistency index of the algal slurry (8.6485×10^{-2} Pa·s^n); n is the rheological index of the algal slurry (0.48).

In Equation (7), the specific heat capacity of the algal slurry c_p (kJ·kg^{-1}·K^{-1}) is expressed as follows:

$$c_p = c_{p,s}\omega + c_{p,f}(1-\omega) \tag{13}$$

where $c_{p,s}$ is the specific heat capacity of the microalgae powder (1.620 kJ·kg^{-1}·K^{-1}); $c_{p,f}$ is the specific heat capacity of the water [37]. According to Equation (13), the value of c_p was set as 3.9186 kJ·kg^{-1}·K^{-1} in this study.

In Equation (7), the thermal conductivity of the algal slurry λ (W·m^{-1}·K^{-1}) is set according to the reference [25].

In Equation (8), the diffusion coefficients of several components D_i (i = 0–5) are 1×10^{-9} m^2·s^{-1} [22]. Based on the HTL kinetics model of microalgae biomass (shown in Figure 2) [22], the reaction rates of all components in the slurry r_i (i = 0–5) were calculated by Equations (14)–(19). *Nannochloropsis* sp. was selected as the studied species. The initial mass fractions of protein, carbohydrate and lipid of microalgae biomass were 5.6 wt.%, 1.3 wt.% and 2.0 wt.%, respectively [38].

$$r_0 = dw_0/dt = -(k_{1p} + k_{2p})w_0 \tag{14}$$

$$r_1 = dw_1/dt = -(k_{1c} + k_{2c})w_1 \tag{15}$$

$$r_2 = dw_2/dt = -(k_{1l} + k_{2l})w_2 \tag{16}$$

$$r_3 = dw_3/dt = k_{1p}w_0 + k_{1c}w_1 + k_{1l}w_2 + k_3w_4 - (k_4 + k_5)w_3 \tag{17}$$

$$r_4 = dw_4/dt = k_{2p}w_0 + k_{2c}w_1 + k_{2l}w_2 + k_4w_3 - (k_3 + k_6)w_4 \tag{18}$$

$$r_5 = dw_5/dt = k_5w_3 + k_6w_4 \tag{19}$$

where k_0–k_6 are reaction rate constants (s^{-1}) [16]:

$$k_i = A_i e^{-Ea/RT} \tag{20}$$

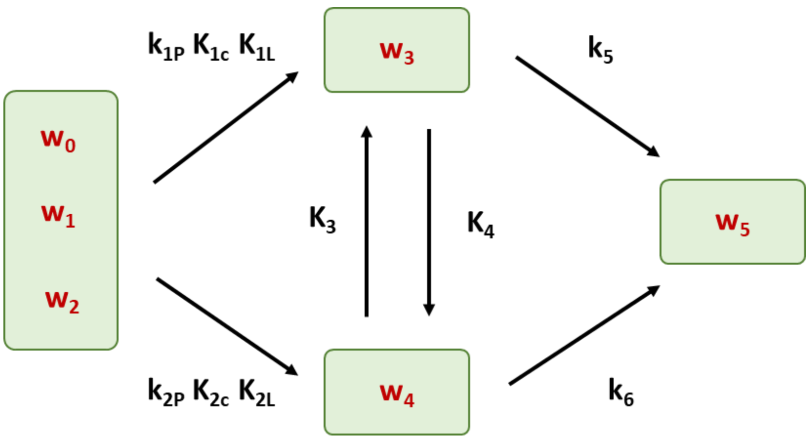

Figure 2. Reaction pathways for HTL of microalgae biomass [38].

2.3. Numerical Method

In the current simulation, a fluid region and a solid region were included in the numerical model (shown in Figure 3), and the grids of computational regions were created in GAMBIT. The solid region is the area of a circular tube, 3 grids were divided in the radial direction, 50 grids were divided in the circumferential direction and 3000 grids were divided in the radial direction. The fluid region is the area of algal slurry, which represents the cylindrical region of the tube channel except the static mixer. In it, 50 grids were divided in the circumferential direction, 28 grids were divided across the width (D_t) of the static mixer, 1 grid was divided across the thickness (δ) of the static mixer. In the fluid region, 4 progressively increasing hexahedral grids were set for calculating the physical field of velocity, temperature and concentration clearly. The first mesh size was set as 0.1 mm, and mesh size was increased by a multiple of 1.2. In the fluid region, the boundary layer region was divided by hexahedral mesh, and other region was divided by tetrahedral mesh. The total mesh number used in this study was 14,066,514.

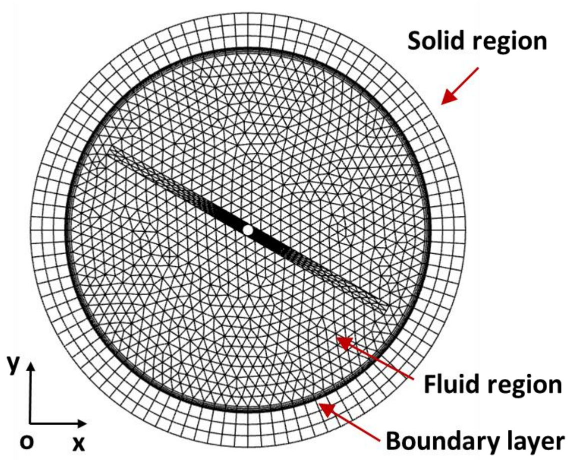

Figure 3. Grid of the solar-driven reactor with static mixer in cross-section.

In the current simulation, the computational software ANSYS FLUENT was utilized for solving this problem. The governing equations were discretized by the finite volume method (FVM). At a Peclet number of algal slurry between 1870 and 4523, the second-order upwind and central differencing schemes were used to approximate the convective and diffusion terms in the differential equation, respectively. The velocity–pressure coupled equation was solved in the collocated grid by using the SIMPLE algorithm. The residuals were detected to check the convergence. The residuals of the continuity equation and other equations were set as 10^{-3} and 10^{-6}, respectively.

The flow resistance f is defined as follows:

$$f = \frac{2d_i}{l\rho u^2}\Delta P \tag{21}$$

where d_i is the inner diameter of the solar-driven tubular tube, l is the length of the solar-driven tubular reactor, ΔP is the differential pressure between the inlet and outlet of the solar-driven tubular reactor.

The Nusselt number Nu of the algal slurry in the solar-driven reactor is expressed as:

$$Nu = \frac{hd_i}{\lambda} \tag{22}$$

where h is the convective heat transfer coefficient ($W \cdot m^{-2} \cdot k^{-1}$):

$$h = \frac{Q}{A\Delta T_m} \tag{23}$$

Q is the heat flux (W):

$$Q = mc_p(T_{out} - T_{in}) \tag{24}$$

The mean temperature difference (ΔT_m) between the inner wall of the reactor and algal slurry is expressed as follows:

$$\Delta T_m = T_w - T_f \tag{25}$$

where T_w is the average temperature of the tube wall, T_f is the mean temperature of fluid in the solar-driven tubular reactor.

The heat transfer enhancement factor PEC is expressed as follows:

$$\mathrm{PEC} = (Nu/Nu_0)/(f/f_0)^{1/3} \tag{26}$$

The yields of the organics Y_i are represented as follows:

$$Y_i = \frac{w_{i,out} - w_{i,in}}{\omega} \tag{27}$$

where w_i is the mean mass fraction of organics at the inlet and outlet of the tube.

The conversion rates of components are represented as follows:

$$R_i = \frac{\rho(w_{i,out} - w_{i,in})}{L/u_m} \tag{28}$$

The Reynolds number *Re* is defined as:

$$Re = \rho u_m L_H/\mu \tag{29}$$

where L_H is the hydraulic length:

$$L_H = d_i - 4A_D/\chi \tag{30}$$

3. Results and Discussion

3.1. Grid Independence and Model Validation

The grid independence has been validated in the case of a solar-driven tubular reactor with a static mixer with a twist ratio of 4. The test case was set at the flow rate of 60 L/h and the direct solar radiation intensity of 750 W/m^2. In Table 2, the convective heat transfer coefficient h, pressure drop ΔP and biocrude yield Y_{BC} have been compared under the same model with four meshes (7.6, 10.2, 14.1, 26.1 million). In addition, the detailed line grids are listed in Table 3.

Table 2. Grid independence of research models.

Grid Number	ΔP (Pa)	ΔP Error (%)	h (W·m^{-2}·k^{-1})	h Error (%)	Y_{BC}	Y_{BC} Error (%)
7642715	358.2	−1.06%	150.8	41.88%	14.7%	−15.84%
10239632	361.0	−0.28%	122.3	15.05%	16.2%	−7.23%
14066514	362.0	Baseline	106.3	Baseline	17.4%	Baseline
26082444	363.5	0.42%	112.3	5.65%	18.5%	6.29%

Table 3. Grid meshing of lines in the model of solar-driven tubular reactor.

Mesh	l	C	δ	D_t
No.1 (7,642,715)	2000	40	1	20
No.2 (10,239,632)	2400	50	1	28
No.3 (14,066,514)	3000	50	1	28
No.4 (26,082,444)	4000	60	1	28

The validated results show that all cases have a similar ΔP, whose ΔP error is below 1.06%. Comparing the h of No.1 and No.2 to No.3, the h errors were 41.88% and 15.05%. Additionally, the h error between the results of 7,642,715 grids and 10,239,632 grids is 5.65%, whose error was below 10%. The lowest biocrude yield Y_{BC} error was also calculated in the meshes between No.3 and No.4. Thus, the model with 14.1 million grids was selected in this simulation.

The reliability of the numerical results of flow resistance, heat transfer and HTL conversion were compared to experiment data. The flow resistance of microalgae in cold conditions obeys the Darcy friction factor [39,40]. The difference between the numerical data and theoretical value was under 10% (Figure 4A). The outlet temperature of algal slurry obtained by experimental data and numerical data was compared to validate the heat transfer. The calculated outlet temperatures of algal slurry in a plain solar-driven reactor were compared with experimental data at 40, 50 and 60 L/h [17], whose errors were 26%, 17.7% and 15%, respectively (Figure 4B). In addition, the reliability of the numerical procedure for simulating the HTL of algal biomass in a continuous reactor has been validated in a previous investigation [24]. The outlet concentration of biocrude obtained by experimental data and numerical data was compared to validate the products from the hydrothermal process.

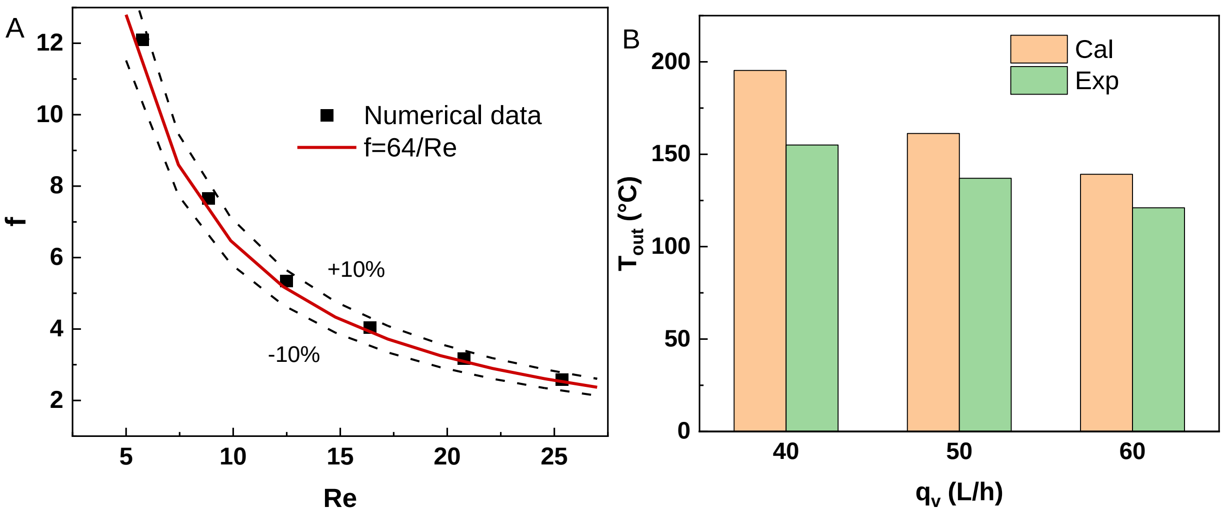

Figure 4. (**A**) Friction factor and (**B**) outlet temperature of algal slurry in a plain solar-driven reactor with various static mixers.

3.2. Flow Resistance of Algal Slurry in the Reactor with Static Mixer

Figure 5A shows the friction factor of the algal slurry flow through the solar-driven reactor with various static mixers, whose twist ratio of the static swirls ranged from 0 to 10. The friction factor of the microalgae flow through the solar-driven reactor significantly decreased with the increasing *Re* from 5 to 25. At a certain *Re*, the friction factor of SM-3 was slightly higher than that of SM-6, SM-10 and SM-0. This phenomenon revealed that the friction-loss-inducing static mixer inserted in the solar-driven reactor was acceptable.

Figure 5B shows the pressure drop of the algal slurry in the solar-driven reactor with various static mixers. The pressure drop obviously increased with the increasing flow rate from 30 to 80 L/h. Thus, flow rate was a key influence factor on the pressure drop in the solar-driven reactor. Additionally, the pressure drop was decreased with the twist ratio from 3 to 10. For instance, the pressure drop in SM-3 (376 Pa) was 1.07, 1.09 times that in SM-6 and SM-10 at the flow rate of 60 L/h, respectively. The results indicated that the static mixer with low twist tape was able to induce a stronger swirling effect, promoting the pressure drop of the algal slurry flow through the solar-driven reactor. Contour plots of average velocity of the algal slurry in SM-0 and SM-3 at 60 L/h are shown in Figure 6.

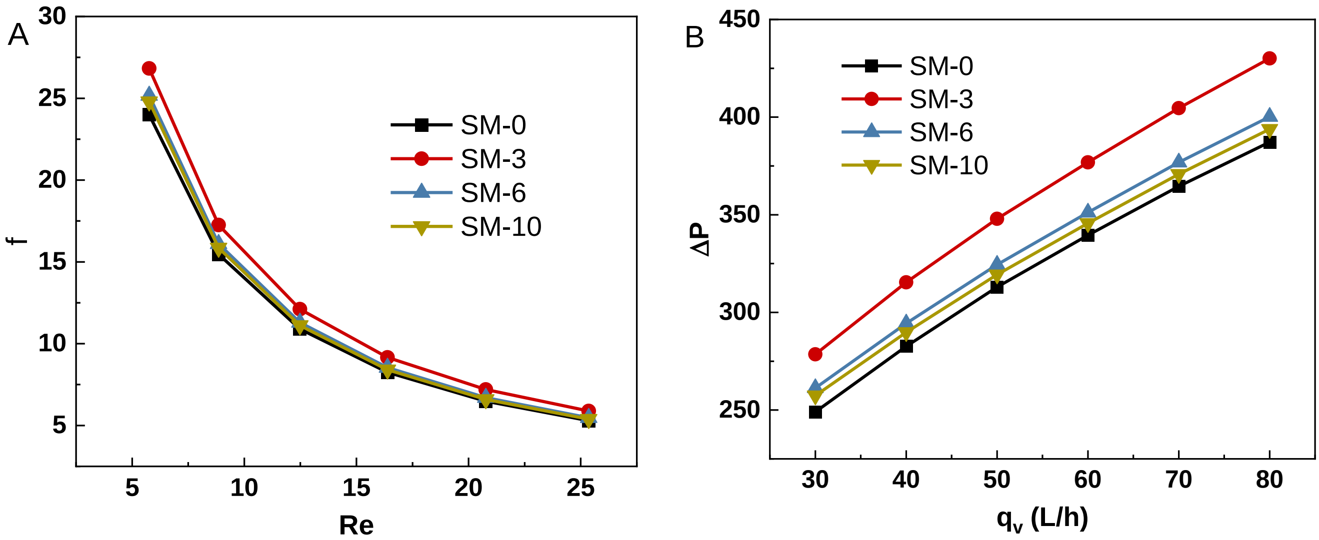

Figure 5. (**A**) Friction factor and (**B**) pressure drop of algal slurry in solar-driven reactor with various static mixers.

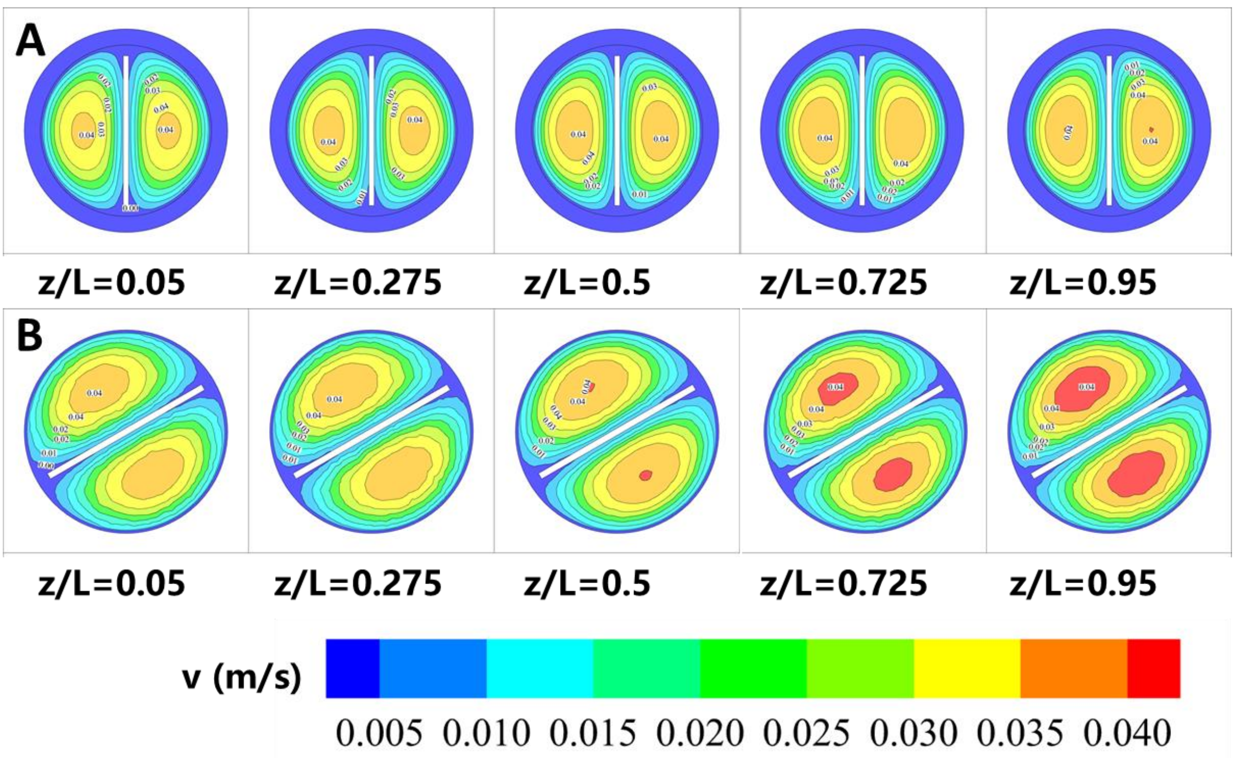

Figure 6. (**A**) Average velocity distribution of the algal slurry in (**A**) SM-0 and (**B**) SM-3 at 60 L/h.

3.3. Heat Transfer Enhancement of Algal Slurry by Static Mixer

Figure 7A shows that the *Nu* of the algal slurry increased with the increase in *Re* from 5 to 25. Particularly, the growth slope of *Nu* in the solar-driven reactor with a static mixer was obviously higher than that of the solar-driven reactor without a static mixer. For instance, the *Nu* increased from 2.04 to 2.72 with the *Re* from 5 to 25 in SM-0, while the *Nu* increased from 3.37 to 6.03 with the *Re* from 5 to 25 in SM-3. It indicated that the swirl effect induced by the static mixer was enhanced by the increasing flow rate. In addition, the *Nu* of the algal slurry in the solar-driven reactor decreased with the increasing twist ratio of the static mixer at a certain *Re*. For example, the *Nu* of SM-3, SM-6 and SM-10 were 6.03, 5.67 and 5.45 at the *Re* of 25, respectively.

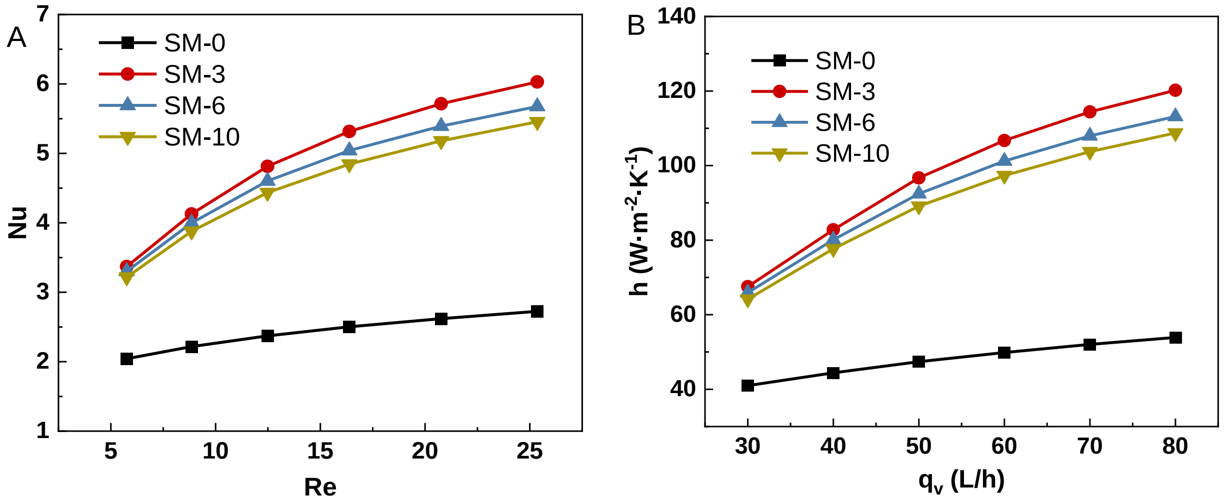

Figure 7. (**A**) *Nu* and (**B**) *h* of algal slurry flow through solar-driven reactor with various static mixers.

Figure 7B shows the *h* increased with the increasing *Re* from 5 to 25. At a certain flow rate, the *h* of the solar-driven reactor with a static mixer was significantly higher than that of the solar-driven reactor without a static mixer. For example, the *h* of the algal slurry in SM-3 (97 $W \cdot m^{-2} \cdot K^{-1}$) was 2.06 times that of SM-0 (47 $W \cdot m^{-2} \cdot K^{-1}$) at the flow rate of 50 L/h. It indicated that the swirling effect induced by the static mixer obviously enhanced the heat transfer performance of the algal slurry in the solar-driven reactor, while the swirling effect was enhanced by the increased of flow rate. In addition, the maximum *h* was observed in the solar-driven reactor with SM-3. For example, the *h* in SM-3 (120 $W \cdot m^{-2} \cdot K^{-1}$) was 1.06 and 1.10 times that of SM-6 and SM-10 at 80 L/h, respectively.

Figure 8 shows the variation of comprehensive heat transfer performance (PEC) with the increasing *Re*. It can be observed that the PEC significantly increased when the *Re* increased from 5 to 25. For example, the PEC of SM-3 increased from 1.59 to 4.71, implying that the static mixer inserted in the solar-driven reactor has a desired effect in the heat transfer enhancement. Figure 9 shows temperature distribution of the algal slurry and in SM-0 and SM-3 at 60 L/h. The temperature distribution of the algal slurries in SM-3 was more uniform than that of SM-0. Therefore, the static mixer was regarded as ideal equipment to enhance the heat transfer in the solar-driven tubular reactor.

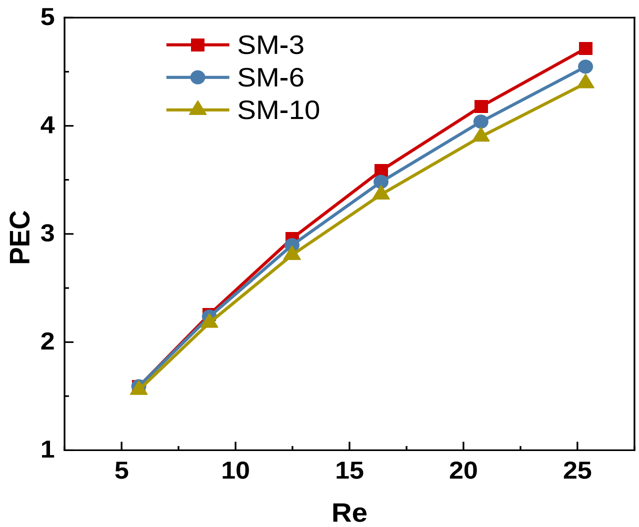

Figure 8. Comprehensive heat transfer performance of solar-driven reactor with inserted static mixers.

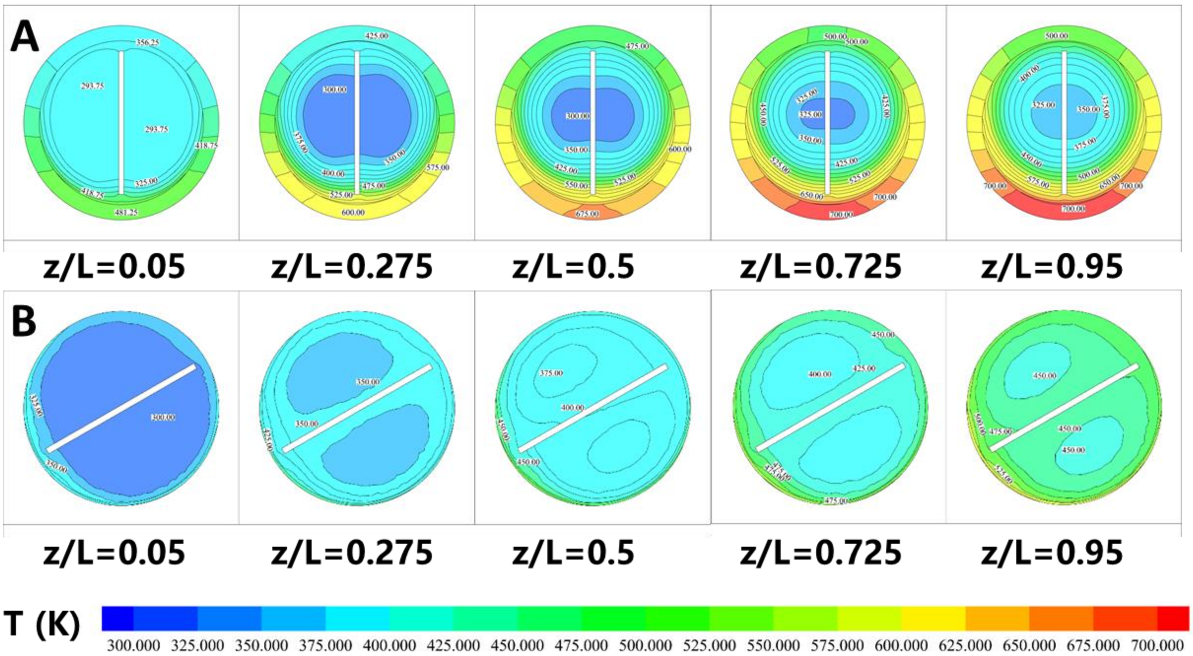

Figure 9. Temperature distribution of the flow cross-section in (**A**) SM-0 and (**B**) SM-3 at 60 L/h.

3.4. *Effect of Swirl Flow Induced by Static Mixer on HTL of Microalgae Biomass*

The static mixer installed in the solar-driven reactor not only promotes the heat transfer of algal slurry but also promotes the production of HTL products. Figure 10 shows the yield of water-soluble organics, biocrude and biogas by the solar-driven reactor in SM-0, SM-3 and SM-6, respectively. Compared to the yield of aqueous organics (21.4%) and biocrude (25.0%), the biogas yield (7.81×10^{-4}%) was negligible.

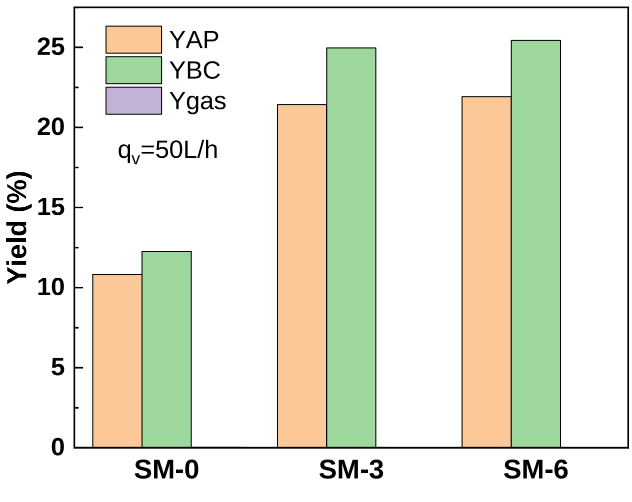

Figure 10. The yield of water-soluble organics, biocrude and biogas in solar-driven reactor with different static mixers.

Figure 11A shows the biocrude yield of the reaction fluid at the outlet section in SM-0, SM-3, SM-6 and SM-10 (30–70 L/h) and the direct solar radiation intensity of 750 W/m^2. The biocrude yields in solar-driven reactors with static mixers were higher than that in SM-0. For example, the biocrude yield in SM-3 (25%) was 2.03 times that in SM-0 (12.3%) at the flow rate of 50 L/h. These results are attributed to the uniform temperature distribution and mass distribution in the solar-driven reactor, which was caused by the swirl effect, shown in Figures 9 and 12. Figure 11B shows the formation rate of organics was promoted at the low flow rate. The maximum formation rate of biocrude (0.074 $g \cdot L^{-1} \cdot s^{-1}$) appeared in the flow rate of 50 L/h. It shows that the swirl effect promoted the production of HTL products in the region of low flow rate through the enhancement of heat transfer. And then, the reduction of temperature limited the production of HTL products in the region of high flow rate.

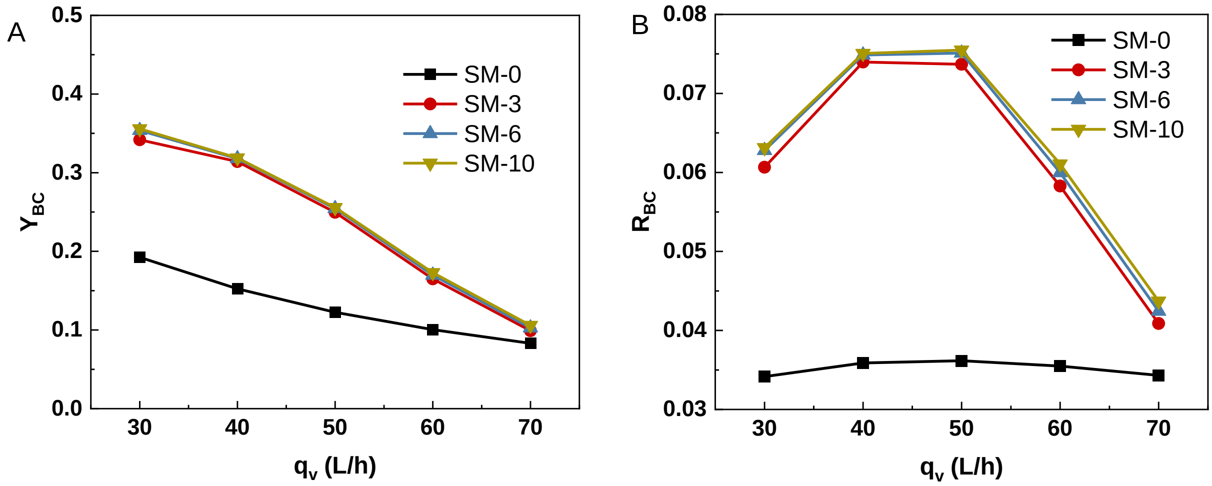

Figure 11. Effect of the static mixer on the (**A**) Y_{BC} and (**B**) R_{BC} in solar-driven reactor.

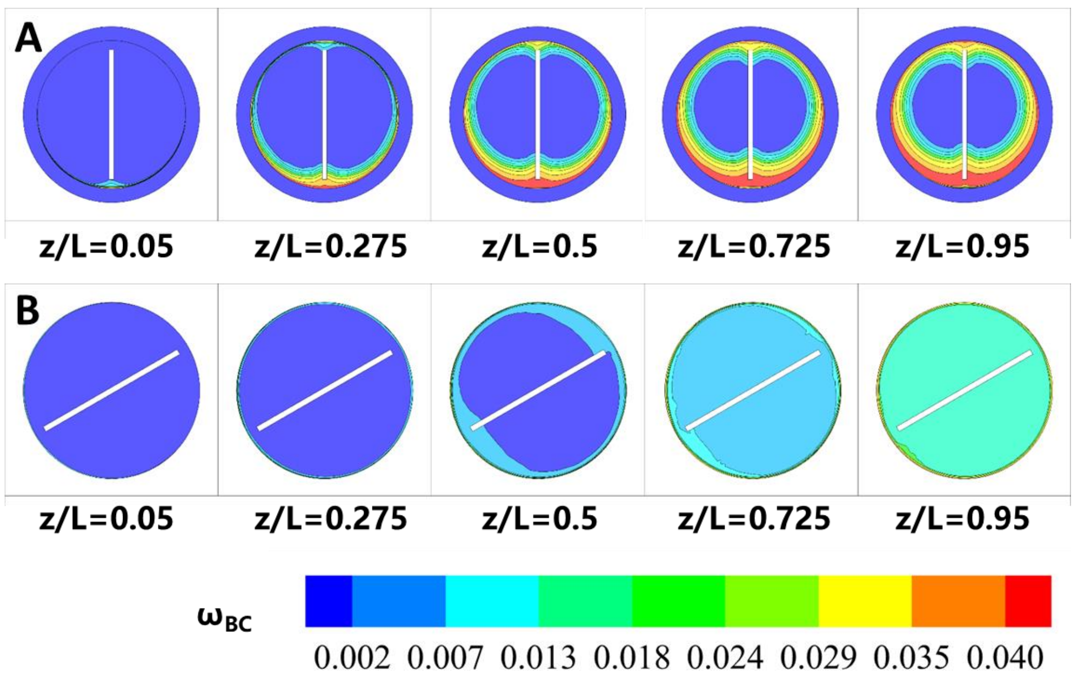

Figure 12. Mass fraction distribution of the flow cross-section in (**A**) SM-0 and (**B**) SM-3 at 60 L/h.

3.5. Effect of Solar Radiation on the HTL in Solar-Driven Reactor

Figure 13 shows the yields of water-soluble organics, biocrude and biogas by the solar-driven reactor at 650, 750 and 850 W/m^2, respectively. Owing to the photothermal transformation, the yields of water-soluble organics and biocrude increased with the increase in direct solar radiation from 650 to 850 W/m^2. The variations of the biocrude yield under various direct solar radiation levels (650, 750, 850 W/m^2) have been shown in Figure 14A. Figure 14B shows the R_{BC} increased with the direct solar radiation from 650 to 850 W/m^2. The formation rate of biocrude at 850 W/m^2 and 50 L/h (0.091 $g \cdot L^{-1} \cdot s^{-1}$) was 1.44 and 1.14 times that of 650 and 750 W/m^2, respectively. At 750 and 850 W/m^2, the optimal conversion rate of biocrude occurred at 50 L/h, whose values were 7.97 and 9.12 g·L^{-1}·s^{-1}, respectively. At 650 W/m^2, the optimal formation rate was 7.33 g·L^{-1}·s^{-1} at 40 L/h. This phenomenon indicated that high thermal energy input guaranteed the high formation rate of algal biomass in the solar-driven reactor.

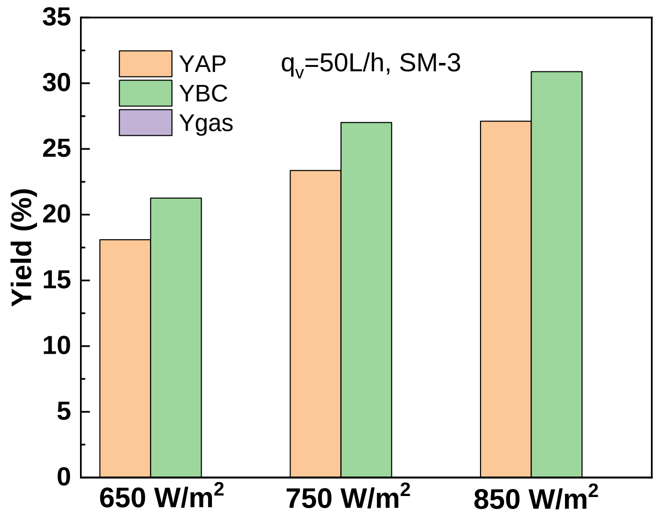

Figure 13. The yield of water-soluble organics, biocrude and biogas in solar-driven reactor with different direct solar radiation levels.

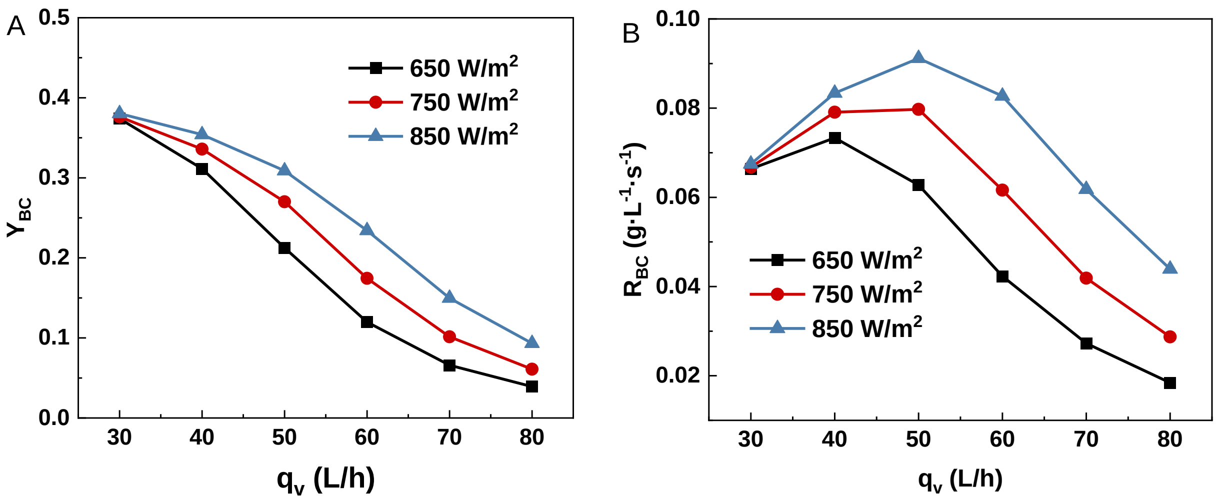

Figure 14. Effect of solar radiation on the (**A**) Y_{BC} and (**B**) R_{BC} in SM-3.

4. Conclusions

In this investigation, the flow, heat transfer and HTL of algal slurry flow through a parabolic solar collector with static mixers (5 < *Re* < 25) were studied. A CFD model combining HTL kinetics and non-uniform heat boundary conditions was established. The static mixer in the solar-driven reactor can cause circumferential flow, significantly increasing the h from 47 to 97 W·m^{-2}·K^{-1}. The static mixer with the twist ratio of 3 (SM-3) had the highest PEC. In the solar-driven reactor, the aqueous organics and biocrude were the main products, and the production of biogas can be ignored. Particularly, the formation rate of organics was dependent on the outlet temperature and the uniformity of the temperature distribution. The R_{BC} was firstly enhanced by the swirl effect and convective effect below 50 L/h but reduced by temperature at the higher flow rate.

Author Contributions: Writing—original draft preparation, H.C.; Writing—review and editing, F.L.; Project administration, H.C.; Resources, X.Z.; Validation, C.S.; Conceptualization, W.P.; Supervision, S.W. All authors have read and agreed to the published version of the manuscript.

Funding: This research was funded by National Natural Science Foundation of China, 52106091.

Data Availability Statement: The data presented in this study are available on request from the corresponding author.

Conflicts of Interest: The authors declare no conflict of interest.

Nomenclature

Symbols	
A	Heat transfer area (m^2)
A_i	Arrhenius constant (s^{-1})
c_p	Specific heat capacity ($kJ \cdot kg^{-1} \cdot K^{-1}$)
D	Diffusivities of all species ($m^2 \cdot s^{-1}$)
d	Diameter of tube (m)
E_a	Activation energy ($kJ \cdot mol^{-1}$)
f	Flow resistance
h	Convective heat transfer coefficient ($W \cdot m^{-2} \cdot K^{-1}$)
k	Reaction rate constant (s^{-1})
L	Length of the tube (m)
Nu	Nusselt number
P	Pressure (Pa)
Pe	Peclet number
PEC	Heat transfer enhancement factor
q	Heat flux (W/m^2)
R	Gas constant ($J \cdot mol^{-1} \cdot K^{-1}$)
R_i	Conversion rate of organics ($g \cdot L^{-1} \cdot s^{-1}$)
Re	Reynolds number
r	Reaction rates of organics ($g \cdot L^{-1} \cdot s^{-1}$)
T	Temperature (K)
ΔT_m	Mean temperature difference (K)
t	Residence time (s)
u	Velocity ($m \cdot s^{-1}$)
u_m	Average velocity ($m \cdot s^{-1}$)
w	Mass fraction of organics
Y	The yield of organics
x	X-direction distance of the tube (m)
y	Y-direction distance of the tube (m)
z	Axial position of the tube (m)
Greek symbols	
ρ	Density ($kg \cdot m^{-3}$)
λ	Thermal conductivity ($W \cdot m^{-1} \cdot K^{-1}$)
μ	Viscosity ($Pa \cdot s$)
ω	Mass fraction of microalgae biomass
γ	Shear rate (s^{-1})
Subscripts	
BC	Biocrude
f	Liquid phase
i	Number of organics in HTL pathways
in	Inlet
out	Outlet
s	Solid phase
w	Tube wall

References

1. Elliott, D.C.; Biller, P.; Ross, A.B.; Schmidt, A.J.; Jones, S.B. Hydrothermal liquefaction of biomass: Developments from batch to continuous process. *Bioresour. Technol.* **2015**, *178*, 147–156. [CrossRef] [PubMed]
2. Hoang, A.T.; Ong, H.C.; Fattah, I.M.R.; Chong, C.T.; Cheng, C.K.; Sakthivel, R.; Ok, Y.S. Progress on the lignocellulosic biomass pyrolysis for biofuel production toward environmental sustainability. *Fuel Process. Technol.* **2021**, *223*, 106997. [CrossRef]
3. Li, S.; Li, X.; Ho, S.H. Microalgae as a solution of third world energy crisis for biofuels production from wastewater toward carbon neutrality: An updated review. *Chemosphere* **2022**, *291 Pt 1*, 132863. [CrossRef] [PubMed]
4. Cronin, D.; Schmidt, A.J.; Billing, J.; Hart, T.R.; Fox, S.P.; Fonoll, X.; Norton, J.; Thorson, M.R. Comparative Study on the Continuous Flow Hydrothermal Liquefaction of Various Wet-Waste Feedstock Types. *ACS Sustain. Chem. Eng.* **2021**, *10*, 1256–1266. [CrossRef]
5. Chen, H.; Xia, A.; Zhu, X.; Huang, Y.; Zhu, X.; Liao, Q. Hydrothermal hydrolysis of algal biomass for biofuels production: A review. *Bioresour. Technol.* **2022**, *344 Pt B*, 126213. [CrossRef]
6. Chen, W.-H.; Lin, B.-J.; Huang, M.-Y.; Chang, J.-S. Thermochemical conversion of microalgal biomass into biofuels: A review. *Bioresour. Technol.* **2015**, *184*, 314–327. [CrossRef] [PubMed]
7. Osman, A.I.; Mehta, N.; Elgarahy, A.M.; Al-Hinai, A.; Al-Muhtaseb, A.A.H.; Rooney, D.W. Conversion of biomass to biofuels and life cycle assessment: A review. *Environ. Chem. Lett.* **2021**, *19*, 4075–4118. [CrossRef]
8. Gollakota, A.; Savage, P.E. Fast and Isothermal Hydrothermal Liquefaction of Polysaccharide Feedstocks. *ACS Sustain. Chem. Eng.* **2020**, *8*, 3762–3772. [CrossRef]
9. Ghavami, N.; Özdenkçi, K.; Chianese, S.; Musmarra, D.; De Blasio, C. Process simulation of hydrothermal carbonization of digestate from energetic perspectives in Aspen Plus. *Energy Convers. Manag.* **2022**, *270*, 116215. [CrossRef]
10. Liu, H.; Basar, I.A.; Eskicioglu, C. Hydrothermal liquefaction for sludge-to-energy conversion: An evaluation of biocrude production and management of waste streams. *Energy* **2023**, *281*, 128268. [CrossRef]
11. Liu, H.; Zhu, Y.; Yang, W.; Li, Y.; Yang, H.; Chen, Y.; Wang, X.; Chen, H. Valorization of the microalgae fixing CO_2 from flue gas by co-hydrothermal liquefaction with high-protein microalgae: Denitrogenation of bio-oil by ash and high energy recovery. *Fuel* **2023**, *340*, 127566. [CrossRef]
12. Ağbulut, Ü.; Sirohi, R.; Lichtfouse, E.; Chen, W.-H.; Len, C.; Show, P.L.; Le, A.T.; Nguyen, X.P.; Hoang, A.T. Microalgae bio-oil production by pyrolysis and hydrothermal liquefaction: Mechanism and characteristics. *Bioresour. Technol.* **2023**, *376*, 128860. [CrossRef]
13. Cheng, F.; Cui, Z.; Mallick, K.; Nirmalakhandan, N.; Brewer, C.E. Hydrothermal liquefaction of high- and low-lipid algae: Mass and energy balances. *Bioresour. Technol.* **2018**, *258*, 158–167. [CrossRef]
14. Ayala-Cortés, A.; Arcelus-Arrillaga, P.; Millan, M.; Arancibia-Bulnes, C.A.; Valadés-Pelayo, P.J.; Villafán-Vidales, H.I. Solar integrated hydrothermal processes: A review. *Renew. Sustain. Energy Rev.* **2021**, *139*, 110575. [CrossRef]
15. Ayala-Cortés, A.; Arcelus-Arrillaga, P.; Millan, M.; Okoye, P.U.; Arancibia-Bulnes, C.A.; Pacheco-Catalán, D.E.; Villafán-Vidales, H.I. Solar hydrothermal processing of agave bagasse: Insights on the effect of operational parameters. *Renew. Energy* **2022**, *192*, 14–23. [CrossRef]
16. Sheehan, J.D.; Savage, P.E. Modeling the effects of microalga biochemical content on the kinetics and biocrude yields from hydrothermal liquefaction. *Bioresour. Technol.* **2017**, *239*, 144–150. [CrossRef]
17. Xiao, C.; Liao, Q.; Fu, Q.; Huang, Y.; Chen, H.; Zhang, H.; Xia, A.; Zhu, X.; Reungsang, A.; Liu, Z. A solar-driven continuous hydrothermal pretreatment system for biomethane production from microalgae biomass. *Appl. Energy* **2019**, *236*, 1011–1018. [CrossRef]
18. Ischia, G.; Orlandi, M.; Fendrich, M.A.; Bettonte, M.; Merzari, F.; Miotello, A.; Fiori, L. Realization of a solar hydrothermal carbonization reactor: A zero-energy technology for waste biomass valorization. *J. Environ. Manag.* **2020**, *259*, 110067. [CrossRef]
19. Giaconia, A.; Turchetti, L.; Ienna, A.; Mazzei, D.; Schiavo, B.; Scialdone, O.; Caputo, G.; Galia, A. Conceptual study of the coupling of a biorefinery process for hydrothermal liquefaction of microalgae with a concentrating solar power plant. In *AIP Conference Proceedings*; AIP Publishing: New York, NY, USA, 2017.
20. Narvaez Saucedo, M.E.; Arancibia-Bulnes, C.A.; Macias, J.D.; Ramirez-Cabrera, M.A.; Valades-Pelayo, P.J. Heat transfer and chemical kinetics analysis of a novel solar reactor for hydrothermal processing. *Solar Energy* **2022**, *241*, 372–385. [CrossRef]
21. Briongos, J.V.; Taramona, S.; Gómez-Hernández, J.; Mulone, V.; Santana, D. Solar and biomass hybridization through hydrothermal carbonization. *Renew. Energy* **2021**, *177*, 268–279. [CrossRef]
22. Ranganathan, P.; Savithri, S. Computational Fluid Dynamics simulation of hydrothermal liquefaction of microalgae in a continuous plug-flow reactor. *Bioresour. Technol.* **2018**, *258*, 151–157. [CrossRef]
23. Xiao, C.; Liao, Q.; Fu, Q.; Huang, Y.; Xia, A.; Chen, H.; Zhu, X. Numerical investigation of laminar mixed convection of microalgae slurry flowing in a solar collector. *Appl. Therm. Eng.* **2020**, *175*, 115366. [CrossRef]
24. Chen, H.; Zhang, X.; Fan, X.; Li, Z.; Qian, L.; Zhang, B.; Wang, S. Convective enhancement of microalgae slurry in continuous tubular reactors for biocrude production during hydrothermal liquefaction. *Appl. Therm. Eng.* **2023**, *220*, 119725. [CrossRef]
25. Chen, H.; Liao, Q.; Fu, Q.; Huang, Y.; Xia, A.; Xiao, C.; Zhu, X. Convective heat transfer characteristics of microalgae slurries in a circular tube flow. *Int. J. Heat Mass Transfer* **2019**, *137*, 823–834. [CrossRef]
26. Chu, W.-X.; Tsai, C.-A.; Lee, B.-H.; Cheng, K.-Y.; Wang, C.-C. Experimental investigation on heat transfer enhancement with twisted tape having various V-cut configurations. *Appl. Therm. Eng.* **2020**, *172*, 115148. [CrossRef]

27. Taheran, E.; Javaherdeh, K. Experimental investigation on the effect of inlet swirl generator on heat transfer and pressure drop of non-Newtonian nanofluid. *Appl. Therm. Eng.* **2019**, *147*, 551–561. [CrossRef]
28. Klemeš, J.J.; Wang, Q.-W.; Varbanov, P.S.; Zeng, M.; Chin, H.H.; Lal, N.S.; Li, N.-Q.; Wang, B.; Wang, X.-C.; Walmsley, T.G. Heat transfer enhancement, intensification and optimisation in heat exchanger network retrofit and operation. *Renew. Sust. Energy Rev.* **2020**, *120*, 109644. [CrossRef]
29. Feng, Z.; Ai, X.; Wu, P.; Lin, Q.; Huang, Z. Experimental investigation of laminar flow and heat transfer characteristics in square minichannels with twisted tapes. *Int. J. Heat Mass Transf.* **2020**, *158*, 119947. [CrossRef]
30. Chen, H.; Fu, Q.; Liao, Q.; Zhang, H.; Huang, Y.; Xia, A.; Zhu, X. Rheological properties of microalgae slurry for application in hydrothermal pretreatment systems. *Bioresour. Technol.* **2018**, *249*, 599–604. [CrossRef]
31. Singh, S.K.; Kacker, R.; Chaurasiya, P.K.; Gautam, S.S. Correlations on heat transfer rate and friction factor of a rectangular toothed v-cut twisted tape exhibiting the combined effects of primary and secondary vortex flows. *Int. Commun. Heat Mass Transf.* **2022**, *139*, 106503. [CrossRef]
32. Varun; Garg, M.O.; Nautiyal, H.; Khurana, S.; Shukla, M.K. Heat transfer augmentation using twisted tape inserts: A review. *Renew. Sustain. Energy Rev.* **2016**, *63*, 193–225. [CrossRef]
33. Maluta, F.; Paglianti, A.; Montante, G. A PBM-Based Procedure for the CFD Simulation of Gas–Liquid Mixing with Compact Inline Static Mixers in Pipelines. *Processes* **2023**, *11*, 198. [CrossRef]
34. Cao, Q.; Zhou, J.; Qian, Y.; Yang, S. Three-Dimensional Model on Liquid–Liquid Mass Transfer of the Kenics Static Mixer: Considering Dynamic Droplet Size Distribution. *Ind. Eng. Chem. Res.* **2023**, *62*, 10507–10522. [CrossRef]
35. Mahian, O.; Kolsi, L.; Amani, M.; Estellé, P.; Ahmadi, G.; Kleinstreuer, C.; Marshall, J.S.; Siavashi, M.; Taylor, R.A.; Niazmand, H.; et al. Recent advances in modeling and simulation of nanofluid—Part I: Fundamentals and theory. *Phys. Rep.* **2019**, *790*, 1–48. [CrossRef]
36. Mahian, O.; Kolsi, L.; Amani, M.; Estellé, P.; Ahmadi, G.; Kleinstreuer, C.; Marshall, J.S.; Taylor, R.A.; Abu-Nada, E.; Rashidi, S.; et al. Recent advances in modeling and simulation of nanofluid flows—Part II: Applications. *Phys. Rep.* **2019**, *791*, 1–59. [CrossRef]
37. Wagner, W.; Kretzschmar, H. *International Steam Tables-Properties of Water and Steam Based on the Industrial Formulation IAPWS-IF97: Tables, Algorithms, Diagrams, and CD-ROM Electronic Steam Tables-All of the Equations of IAPWS-IF97 Including a Complete Set of Supplementary Backward Equations for Fast Calculations of Heat Cycles, Boilers, and Steam Turbines*; Springer Science & Business Media: Berlin, Germany, 2007.
38. Valdez, P.J.; Tocco, V.J.; Savage, P.E. A general kinetic model for the hydrothermal liquefaction of microalgae. *Bioresour. Technol.* **2014**, *163*, 123–127. [CrossRef]
39. Brown, T.M.; Duan, P.; Savage, P.E. Hydrothermal Liquefaction and Gasification of *Nannochloropsis* sp. *Energy Fuels* **2010**, *24*, 3639–3646. [CrossRef]
40. Chhabra, R.P.; Richardson, J.F. *Non-Newtonian Flow in the Process Industries*; Butterworth-Heinemann: Oxford, UK, 1999; pp. 147–158.

Disclaimer/Publisher's Note: The statements, opinions and data contained in all publications are solely those of the individual author(s) and contributor(s) and not of MDPI and/or the editor(s). MDPI and/or the editor(s) disclaim responsibility for any injury to people or property resulting from any ideas, methods, instructions or products referred to in the content.